ORCA – Online Research @ Cardiff

This is an Open Access document downloaded from ORCA, Cardiff University's institutional repository:https://orca.cardiff.ac.uk/id/eprint/66819/

This is the author's version of a work that was submitted to / accepted for publication.

Citation for final published version:

Davies, Robert and Jefferson, Anthony 2015. The simulation of inelastic matrix strains in cementitious materials using micromechanical solutions. Engineering Fracture Mechanics 133 10.1016/j.engfracmech.2014.10.010

Publishers page: http://dx.doi.org/10.1016/j.engfracmech.2014.10.01...

Please note:
Changes made as a result of publishing processes such as copy-editing, formatting and page numbers may not be reflected in this version. For the definitive version of this publication, please refer to the published source. You are advised to consult the publisher's version if you wish to cite this paper.

This version is being made available in accordance with publisher policies. See http://orca.cf.ac.uk/policies.html for usage policies. Copyright and moral rights for publications made available in ORCA are retained by the copyright holders.

The simulation of inelastic matrix strains in cementitious materials using micromechanical solutions

Robert Davies*, Anthony Jefferson*

Cardiff School of Engineering, Cardiff University, Cardiff, Wales, United Kingdom, CF24 3AA

Abstract

A new approach is described for simulating inelastic behaviour in the matrix component of a two-phase composite material. Quasi-isotropic distributed micro-cracking, accompanying volumetric matrix changes, is combined with anisotropic micro-cracking arising from directional loading. An exterior point Eshelby solution is used to obtain stress concentrations adjacent to inclusions. The accuracy of these solutions is assessed using a series of three dimensional finite element analyses. A set of stress/ strain paths are considered to illustrate the model's characteristics. The model is then applied to the problem of autogenous shrinkage in a cementitious composite, giving results that compare favourably with experimental data.

Keywords: composite, cementitious, inelastic strain, matrix, micro-cracks

1. Introduction

Micromechanical models allow individual material properties, micro-cracking and inelastic behaviour to be modelled at the particle scale of a composite

*Corresponding author.
Email address: DaviesRE11@cf.ac.uk (Robert Davies)

material. They also provide a means of linking the predicted behaviour to the macro-scale response. This paper describes a model for a two-phase composite material which has a matrix phase and inclusions. The particular focus is on simulating inelastic behaviour in the matrix phase alone (Acker, 2001). Inelastic strains may derive from shrinkage, creep, micro-cracking, differential thermal expansion or ageing. These time dependent phenomena are particularly important when simulating cementitious composite materials such as concrete.

Neville et al. (1983) reviewed a number of two-phase models for creep and shrinkage of concrete, including those of Hirsch (1962), Counto (1964) and England (1965), in which the behaviour of the composite was derived from the properties of the aggregate and cement paste phases. A number of more recent models are based on multi-level schemes in which macro-scale stresses and strains are derived by up-scaling the behaviour at the micro-scale and below. Xi and Jennings (1997) presented a multiscale model for shrinkage in concrete and in cement paste that considered the behaviour from the nano to the meso-scale. Bernard et al. (2003) described the inelastic strains from chemical shrinkage in cementitious composites with a multi-level model and Pichler et al. (2007), also using a multi-level scheme, simulated early age autogenous shrinkage for the same type of cement based material. The latter model was further developed to include up-scaling of creep properties (Pichler and Lackner, 2008). A two level multi-staged model was presented by Scheiner et al. (2009) to describe creep in concrete in which the creep in cement hydrates was considered explicitly. These multi-scale models are particularly successful at simulating the development of strength during cement

hydration (Pichler and Hellmich, 2011).

In cementitious composites, time-dependent inelastic strains are believed to originate in the matrix phase (or matrix-inclusion interface)(van Mier, 1997) and thus it advantageous to be able to explicitly model inelastic behaviour in the separate phases of a composite at the micro-scale. Inelastic strains in inclusions are readily considered with the standard Eshelby (1957) approach and such strains may be added to the eigenstrains arising from a mismatch of elastic properties (Mura, 1987; Weng, 1988; Nemat-Nasser and Hori, 1999). However, if the elastic properties and strains change over time due, for example, to hydration and/or micro-cracking, then methods which consider the non-linear behaviour of the phases are needed.

A general approach for including inelastic strains in one (or more) of the phases of a composite is to linearise the non-linear constitutive equations. Models based on this approach have used incremental tangent moduli (Hill, 1965), secant moduli (Tandon and Weng, 1988; Dunn and Ledbetter, 1997) and second order moduli estimates of the phase constitutive equations (Castaneda, 1996).

Ju and Sun (2001) presented a model for simulating the inelastic behaviour of metal matrix composites in which an effective yield function was derived using a statistical distribution of inclusions.

The method described as 'Transformed Field analysis' (TFA) was conceived by Laws (1973) and further developed by Dvorak and Benveniste (1992), Dvorak (1992) and Chaboche et al. (2001). The method allows the simulation of generally anisotropic behaviour in the phases of a composite at the expense of solving a local nonlinear system.

Recently Monchiet et al. (2012) presented a closed form solution for an orthotropic medium containing arbitrarily orientated cracks.

The inelastic micro-cracking strains arising from early-age volumetric time-dependent phenomena are generally quasi-isotropic in nature and distributed (Hearn, 1999). The micro-cracking (and subsequent macro-cracking) resulting from mechanical loading and/or mechanical restraints are generally anisotropic in nature and arise after material curing, e.g. during the first application of mechanical load. It is this separation that is exploited in the proposed model, which includes two sets of micro-cracking variables, one of which represents distributed isotropic micro-cracking in the matrix and the other of which accounts for anisotropic (or directional) cracking of the composite.

The advantage of the proposed approach is that it avoids the need for a numerical solution to evaluate the Eshelby (or concentration) tensor for a changing generally anisotropic matrix material (Desrumaux et al., 2001).

Although the model presented in this paper does not use a volumetric-deviatoric separation of the stress/strain tensors, there are some similarities with approaches that do use such a separation (Carol et al., 2001; Leukart and Ramm, 2003, 2006; Grassl and Jirasek, 2006).

The paper provides a description of the new constitutive model and the way in which inelastic matrix strains are simulated. Then the theory for including two forms of micro-cracking, associated with early age volumetric matrix changes and directional (anisotropic) loading respectively, is presented.

The approach of Mihai and Jefferson (2011) is used for the initiation and

evolution of both forms of micro-crack. The solutions and homogenisation scheme, upon which the model is based, are validated using finite element simulations for the problem of matrix shrinkage restrained by both a single and by multiple inclusions. A series of illustrative stress/strain paths are used to demonstrate the performance of the model and this is followed by application of the model to the problem of autogenous shrinkage in a cementitious composite including micro-cracking.

2. Constitutive model theory

The two phase composite average stress ($\bar{\boldsymbol{\sigma}}$) and strain ($\bar{\boldsymbol{\varepsilon}}$) tensors are defined by the summations in equations (1) and (2),

$$\bar{\boldsymbol{\sigma}} = f_\Omega \boldsymbol{\sigma}_\Omega + f_M \boldsymbol{\sigma}_M \tag{1}$$

$$\bar{\boldsymbol{\varepsilon}} = f_\Omega \boldsymbol{\varepsilon}_\Omega + f_M \boldsymbol{\varepsilon}_M \tag{2}$$

in which the subscripts M and Ω denote the matrix and inclusion phases respectively. The sum of the volume fractions (f_Ω and f_M) is unity.

Figure 1 shows an idealised two-phase composite with a matrix phase containing spherical inclusions and inelastic strains ($\boldsymbol{\varepsilon}_{IN}$). Micro-cracking is split into two categories, namely volumetric and directional; it being assumed that micro-cracking arising from volumetric strains is quasi-isotropic in nature. Directional, or anisotropic, micro-cracking strains are added to the isotropically micro-cracked composite.

2.1. Elastic two-phase composite

The elastic properties of the two-phase composite are computed using the classical Eshelby (1957) solution and the Mori-Tanaka homogenisation

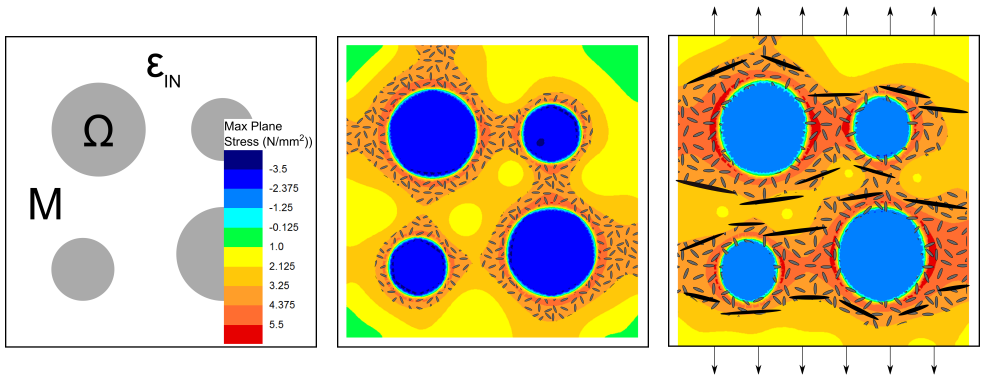

(a) Standard inelastic M and elastic Ω

(b) Isotropic inelastic strain

(c) Isotropic inelastic strain and uniaxial far-field strain

Figure 1: Two-phase composite with illustrative rational

scheme for non-dilute inclusions (Mori and Tanaka, 1973; Benveniste, 1987). The constitutive relationship is shown in equation (3),

$$\bar{\boldsymbol{\sigma}} = \mathbf{D}_{M\Omega} : \bar{\boldsymbol{\varepsilon}}_e \tag{3}$$

where $\mathbf{D}_{M\Omega} = (f_\Omega \mathbf{D}_\Omega \cdot \mathbf{T}_\Omega + f_M \mathbf{D}_M) \cdot \left(f_\Omega \mathbf{T}_\Omega + \mathbf{I}^{4s} f_M\right)^{-1}$, $\mathbf{T}_\Omega = \mathbf{I}^{4s} + \mathbf{S}_\Omega \cdot \mathbf{A}_\Omega$, $\mathbf{A}_\Omega = [(\mathbf{D}_\Omega - \mathbf{D}_M) \cdot \mathbf{S}_\Omega + \mathbf{D}_M]^{-1} \cdot (\mathbf{D}_M - \mathbf{D}_\Omega)$, $\mathbf{D}_M$ and $\mathbf{D}_\Omega$ are the elastic tensors for the matrix and inclusion phases respectively. $\mathbf{S}_\Omega$ is the interior point fourth order Eshelby tensor (Nemat-Nasser and Hori, 1999). $\mathbf{I}^{4s}$ is the fourth order identity tensor and the subscript e denotes elastic.

2.2. A two-phase composite with inelastic strain in the matrix only

In the case where there is an inelastic strain in the matrix ($\boldsymbol{\varepsilon}_{IN}$), the disturbance ($\boldsymbol{\varepsilon}_c$) and eigenstrains ($\boldsymbol{\varepsilon}_\tau$) are given by equations (4) and (5) respectively.

$$\boldsymbol{\varepsilon}_c = \mathbf{S}_\Omega : (\boldsymbol{\varepsilon}_\tau - \boldsymbol{\varepsilon}_{IN}) \tag{4}$$

$$\boldsymbol{\varepsilon}_\tau = \mathbf{A}_\Omega : (\boldsymbol{\varepsilon}_0 - \mathbf{S}_\Omega : \boldsymbol{\varepsilon}_{IN}) \tag{5}$$

in which $\boldsymbol{\varepsilon}_0$ is the farfield strain tensor.

The stress-strain relationships for the phases are given by equations (6) and (7),

$$\boldsymbol{\sigma}_M = \mathbf{D}_M : (\boldsymbol{\varepsilon}_M - \boldsymbol{\varepsilon}_{IN}) \tag{6}$$

$$\boldsymbol{\sigma}_\Omega = \mathbf{D}_\Omega \cdot \mathbf{T}_\Omega : (\boldsymbol{\varepsilon}_M - \mathbf{S}_\Omega : \boldsymbol{\varepsilon}_{IN}) \tag{7}$$

and the overall constitutive equation relationship by equation (8),

$$\bar{\boldsymbol{\sigma}} = \mathbf{D}_{M\Omega} : (\bar{\boldsymbol{\varepsilon}} - \boldsymbol{\varepsilon}_{INEQ}) \tag{8}$$

where $\boldsymbol{\varepsilon}_{INEQ} = \left[\mathbf{D}_{M\Omega}{}^{-1} \left(f_\Omega \mathbf{D}_\Omega \cdot \mathbf{T}_\Omega \cdot \mathbf{S}_\Omega + f_M \mathbf{D}_M\right) - f_\Omega \mathbf{T}_\Omega \cdot \mathbf{S}_\Omega\right] : \boldsymbol{\varepsilon}_{IN}$.

3. Additional strain due to micro-cracks

3.1. Volumetric matrix micro-cracking

The micro-cracking which arises from the volumetric changes in the matrix phase due to shrinkage, creep and early age thermal effects for cementitious composites are considered to be effectively isotropic. Such micro-cracking can be simulated by replacing $\mathbf{D}_M$ with $\mathbf{D}_{M\omega}$, where $\mathbf{D}_{M\omega}$ is defined by,

$$\mathbf{D}_{M\omega} = (1 - \omega_M)\mathbf{D}_M \tag{9}$$

where the volumetric micro-cracking parameter is $\omega_M \in [0, 1]$. The resulting constitutive equation is,

$$\bar{\boldsymbol{\sigma}} = \mathbf{D}_{M\Omega\omega_M} : (\bar{\boldsymbol{\varepsilon}} - \boldsymbol{\varepsilon}_{INEQ\omega_M}) \tag{10}$$

where

$$\boldsymbol{\varepsilon}_{INEQ\omega_M} = \left[\mathbf{D}_{M\Omega\omega_M}{}^{-1}\left(f_\Omega \mathbf{D}_\Omega \cdot \mathbf{T}_{\Omega\omega_M} \cdot \mathbf{S}_\Omega + f_M \mathbf{D}_{M\omega}\right) - f_\Omega \mathbf{T}_{\Omega\omega_M} \cdot \mathbf{S}_\Omega\right] : \boldsymbol{\varepsilon}_{IN}, \tag{11}$$

$$\mathbf{D}_{M\Omega\omega_M} = \left(f_\Omega \mathbf{D}_\Omega \cdot \mathbf{T}_{\Omega\omega_M} + f_M \mathbf{D}_{M\omega}\right) \cdot \left(f_\Omega \mathbf{T}_{\Omega\omega_M} + \mathbf{I}^{4s} f_M\right)^{-1}, \tag{12}$$

$$\mathbf{T}_{\Omega\omega_M} = \mathbf{I}^{4s} + \mathbf{S}_\Omega \cdot \mathbf{A}_{\Omega\omega_M} \tag{13}$$

and

$$\mathbf{A}_{\Omega\omega_M} = \left[\left(\mathbf{D}_\Omega - \mathbf{D}_{M\omega}\right) \cdot \mathbf{S}_\Omega + \mathbf{D}_{M\omega}\right]^{-1} \cdot \left[\mathbf{D}_{M\omega} - \mathbf{D}_\Omega\right]. \tag{14}$$

It is noted that the standard form of Eshelby tensor remains valid with changing degrees of volumetric micro-cracking because $\mathbf{D}_{M\omega}$ retains the isotropic form.

3.2. Directional micro-cracking from mechanical loading

Mechanical loading (and structural restraints) often leads to the development of anisotropic micro-cracks which can develop into macro-cracks. Mihai and Jefferson (2011) employed the Budiansky and O'Connell (1976) solution to represent such micro-cracking but replaced the elastic properties of single phase material in the original paper with effective elastic properties of the composite material. This avoided the need for Eshelby tensors for generally anisotropically cracked media which (other than for specialised cases) require numerical evaluation.

The same approach is now adopted for the isotropically cracked composite. The resulting stress-strain relationship is given by equation (15),

$$\bar{\boldsymbol{\sigma}} = \mathbf{D}_{M\Omega\omega_M} : \left(\bar{\boldsymbol{\varepsilon}} - \boldsymbol{\varepsilon}_{INEQ\omega_M} - \boldsymbol{\varepsilon}_a\right) \tag{15}$$

in which the added strain ($\boldsymbol{\varepsilon}_a$) is now relative to the isotropically micro-cracked composite. This additional strain due to a set of circular cracks with the same orientation is given by equation (16) (Budiansky and O'Connell, 1976),

$$\boldsymbol{\varepsilon}_\alpha = f\frac{16\left(1-{\nu_M}^2\right)}{3E_M}\begin{bmatrix}\boldsymbol{\sigma}_{rr}\\ \frac{4}{2-\nu_M}\boldsymbol{\sigma}_{rs}\\ \frac{4}{2-\nu_M}\boldsymbol{\sigma}_{rt}\end{bmatrix} \tag{16}$$

in which the crack density parameter (f) can also be expressed as a micro-crack variable $\omega_0 \in [0,1]$ (Jefferson and Bennett, 2007), as in equation (17).

$$f = \frac{3}{16\left(1-{\nu_M}^2\right)}\left(\frac{\omega_0}{1-\omega_0}\right) \tag{17}$$

Integrating contributions from all directions around a hemisphere gives the total added strain equation as shown in equation (18). McLaren's integration rule with 29 sample directions is used to evaluate this integration numerically (Stroud, 1972).

$$\boldsymbol{\varepsilon}_a = \left(\frac{1}{2\pi}\int_{2\pi}\int_{\frac{\pi}{2}}\mathbf{N}_\varepsilon\cdot\mathbf{C}_L\cdot\mathbf{N}\cdot\frac{\omega_0(\theta,\psi)}{1-\omega_0(\theta,\psi)}sin(\psi)\mathrm{d}\psi\mathrm{d}\theta\right):\bar{\boldsymbol{\sigma}} \tag{18}$$

in which $\mathbf{N}$ and $\mathbf{N}_\varepsilon$ are the stress and strain transformation tensors. These relationships can be used in (15) to yield the overall constitutive equation (19),

$$\bar{\boldsymbol{\sigma}} = \left(\mathbf{I}^{4s}+\mathbf{D}_{M\Omega\omega_M}\cdot\mathbf{C}_{add}\right)^{-1}\mathbf{D}_{M\Omega\omega_M}:\left(\bar{\boldsymbol{\varepsilon}}-\boldsymbol{\varepsilon}_{INEQ\omega_M}\right) \tag{19}$$

where

$$\mathbf{C}_{add} = \left(\frac{1}{2\pi}\int_{2\pi}\int_{\frac{\pi}{2}}\mathbf{N}_\varepsilon\cdot\mathbf{C}_L\cdot\mathbf{N}\cdot\frac{\omega(\theta,\psi)}{1-\omega(\theta,\psi)}sin(\psi)\mathrm{d}\psi\mathrm{d}\theta\right) \tag{20}$$

$\mathbf{C}_L$ is the elastic compliance (Nemat-Nasser and Hori, 1999).

3.3. Exterior point Eshelby stress outside an inclusion

The exterior point Eshelby solution (Ju and Sun, 1999) is used to give the strain and stress amplification at any point in the matrix as shown in Equations 21 and 22 respectively. The stress tensor in the matrix on each local plane is given by Equation 23.

$$\boldsymbol{\varepsilon}_{M\Omega}(\mathbf{x}) = \mathbf{T}_{E\omega_M}(\mathbf{x}) : \boldsymbol{\varepsilon}_M - \mathbf{T}_{\Omega\omega_M} \cdot \mathbf{S}_E(\mathbf{x}) : \boldsymbol{\varepsilon}_{IN} \tag{21}$$

$$\boldsymbol{\sigma}_{M\Omega}(\mathbf{x}) = \mathbf{D}_{M\omega} : \boldsymbol{\varepsilon}_{M\Omega}(\mathbf{x}) \tag{22}$$

$$s_{M\Omega}(\mathbf{x}) = \mathbf{N} \cdot \boldsymbol{\sigma}_{M\Omega}(\mathbf{x}) \tag{23}$$

where $\mathbf{T}_{E\omega_M}(\mathbf{x})$ and $\mathbf{S}_E(\mathbf{x})$ are the exterior point Eshelby tensors defined by Ju and Sun (1999), see also Mihai and Jefferson (2011). $\mathbf{x}$ is the position vector from the centre of a spherical aggregate particle, $\rho = a/|\mathbf{x}|$ is the relative distance taken as 0.999, $|\mathbf{x}| = \sqrt{x_i x_i}$ is the position vector and a is the radius of the spherical inclusion.

3.4. Micro-crack criterion and evolution

The proposed model requires two micro-crack evolution equations for (i) volumetric micro-cracks which are considered to be controlled by the coarse aggregate particles and (ii) directional micro-cracks (and eventually macro-cracks) which are considered to extend over the coarse aggregate particles.

The measurement of post-peak volumetric tensile behaviour of concrete at low strains is difficult and the authors found little experimental data upon which to base the evolution function directly. However, a volumetric softening function may be chosen by making the following assumptions:

1. The start of micro-cracking is associated with pre-peak nonlinearity in uniaxial tension, which typically occurs at approximately 70% of the peak tensile load (van Mier, 1997),
2. the relative displacement at full softening, in any direction under volumetric loading, is governed by the coarse aggregate particles and
3. this relative displacement is of similar magnitude to that for directional loading.

The above assumptions allow the same function form to be used for both volumetric and directional micro-crack evolution. The equation selected is based on a standard form which was adopted by Mihai and Jefferson (2011), as follows

$$\sigma_\beta = f_{t\beta} e^{-c_\beta \dfrac{u_\beta - u_{t\beta}}{u_{0\beta} - u_{t\beta}}} \tag{24}$$

in which subscript β denotes volumetric (m) or directional (d) micro-cracking, c is a constant taken to be 5, which is appropriate for this type of evolution, $f_{t\beta}$ is a local tensile strength at the aggregate/ cement paste interface and u is a relative displacement across a zone of material size equal to the coarse aggregate particles. The strain at first uniaxial micro-cracking ($\varepsilon_{t\beta}$) is taken as

$$\varepsilon_{t\beta} = \frac{f_{t\beta}}{E_\beta} \tag{25}$$

in which E_M is Young's modulus of the matrix and E_d is Young's modulus of the composite. The local strains in the effectively fully micro-cracked ($\varepsilon_{0\beta}$) state are assumed to be related to the relative displacements by

$$\varepsilon_{0\beta} = \frac{u_{0\beta}}{h_\beta} \tag{26}$$

in which h_m is the size of the coarse aggregate and h_d is assumed to be 3 times the size of coarse aggregate. Coarse aggregate is typically 10mm in diameter for laboratory concrete and 20mm for structural concrete. The relative displacement at the fully micro-cracked case for u_{0m} is taken as 0.1mm whereas u_{0d} is taken as 0.2mm (Walraven and Reinhardt, 1981).

The function described by equation 24, for both the volumetric and directional micro-cracking cases, is illustrated in Figure 2.

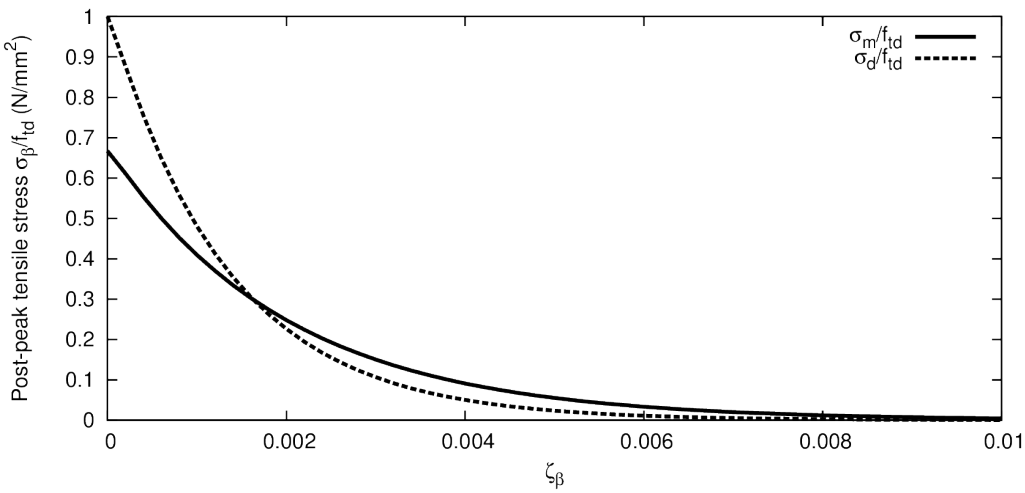

Figure 2: Volumetric and directional tensile softening functions

The onset of micro-cracking is controlled by the elastic stress field. The micro-cracking initiation criterion for the volumetric component is reached when the mean matrix stress reaches the tensile strength of the matrix. The micro-cracking initiation criterion for the directional component is reached when the local principal stress (s_I), given by equation (27), exceeds the initial

interface tensile strength (f_{td}).

$$s_I = s_{rr}\left(\frac{1+\alpha_L}{2}\right) + \sqrt{{s_{rr}}^2\left(\frac{1-\alpha_L}{2}\right)^2 + {\tau_L}^2} \tag{27}$$

where $\alpha_L = \left(\frac{\nu_M}{1-\nu_M}\right)$ and $\tau_L = \sqrt{{s_{rs}}^2 + {s_{rt}}^2}$, in which $s = s_{M\Omega}$ is the transformed amplified stress adjacent to an inclusion (Mihai and Jefferson, 2011), as defined in equation (23).

Once formed, the extent of micro-cracking is expressed in terms of the parameters (ω_β), which are given by

$$\omega_\beta = 1 - \frac{\varepsilon_{t\beta}}{\zeta_\beta} e^{-c_\beta\left(\frac{\zeta_\beta - \varepsilon_{t\beta}}{\varepsilon_{0\beta} - \varepsilon_{t\beta}}\right)} \tag{28}$$

this depends on the effective local strain parameters ζ_m and ζ_d, the former of which is governed by the following volumetric micro-cracking function (29) and the latter by the directional micro-cracking function (30).

$$F_{\zeta_m}(\boldsymbol{\varepsilon}_{mv}, \zeta_m) = \boldsymbol{\varepsilon}_{mv}/3 - \zeta_m \tag{29}$$

$$F_{\zeta_d}(\boldsymbol{\varepsilon}_L, \zeta_d) = \boldsymbol{\varepsilon}_{L_{rr}}\left(\frac{1+\alpha_L}{2}\right) + \sqrt{{\boldsymbol{\varepsilon}_{L_{rr}}}^2\left(\frac{1-\alpha_L}{2}\right)^2 + {r_\zeta}^2\gamma^2} - \zeta_d \tag{30}$$

where $\gamma = \sqrt{{\boldsymbol{\varepsilon}_{L_{rs}}}^2 + {\boldsymbol{\varepsilon}_{L_{rt}}}^2}$ and $r_{\zeta_d} = \left(\frac{\nu_M - 1/2}{\nu_M - 1}\right)$.

The functions are subject to the standard loading/ unloading conditions as follows

$$F_{\zeta_\beta} \leq 0; \qquad \dot{\zeta}_\beta \geq 0; \qquad F_{\zeta_\beta}\dot{\zeta}_\beta = 0 \tag{31}$$

The micro-cracking evolution for the volumetric component is always controlled by the mean local matrix strain. The directional local strain component ($\boldsymbol{\varepsilon}_L$) is assumed equal to the sum of the peak elastic strain in the matrix

phase ($\boldsymbol{\varepsilon}_{LMe}$), based on $\boldsymbol{s}_{M\Omega}$ and the local micro-cracking strain ($\boldsymbol{\varepsilon}_{\alpha}$) (Mihai and Jefferson, 2011), as shown in (32).

$$\boldsymbol{\varepsilon}_L = \boldsymbol{\varepsilon}_{LMe} + \boldsymbol{\varepsilon}_{\alpha} \tag{32}$$

where

$$\boldsymbol{\varepsilon}_{LMe} = (1 - \omega_0)\mathbf{C}_L : \boldsymbol{s}_{M\Omega} \tag{33}$$

and

$$\boldsymbol{\varepsilon}_{\alpha} = \omega_0 \mathbf{N}_{\varepsilon} \cdot \bar{\boldsymbol{\varepsilon}}_e = \omega_0 \mathbf{N}_{\varepsilon} \cdot (\bar{\boldsymbol{\varepsilon}} - \boldsymbol{\varepsilon}_{INEQ\omega_M}) \,. \tag{34}$$

4. FE Validation of homogenised solution

In this section, the accuracy of the proposed approach adopted for homogenisation and stress concentrations is assessed using two three dimensional finite element simulations. These models simulate the free shrinkage of the composite and were carried out using the LUSAS (2012) finite element software. Sun et al. (2007) compared the upper and lower bound of elastic properties using random unit cell finite element models for accuracy against an analytical solution and experimental results for varying inclusion volume fractions. Here, we examine the effect of the exterior point Eshelby amplification for a perfect interface bond. The material properties used for both analyses are given in Table 1.

The first model simulated a spherical inclusion within a matrix where the volumetric shrinkage potential (strain) of 0.0003 was applied to the matrix only. There were 54000 quadratic tetrahedral stress elements in the single inclusion model. Figure 3 compares the numerical and analytical major

Table 1: Material properties used for the FE validation

E_M (N/mm^2)	ν_M	E_Ω (N/mm^2)	ν_Ω
24000	0.15	55000	0.25

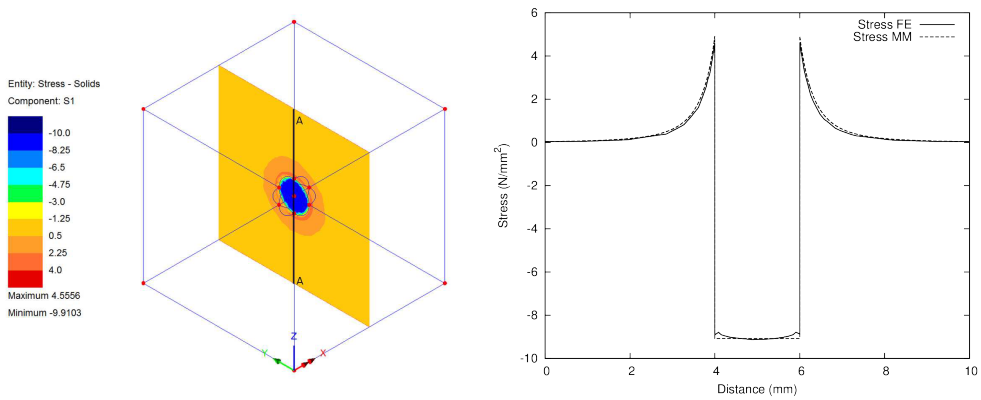

Figure 3: 3D FE plot and stress spatial distribution plot for one inclusion

principal stresses along section A-A. These major principal stresses compare favourably.

The second model contains multiple inclusions to simulate a homogenised composite material. 64 spherical inclusions were placed within a cube of matrix material. In total there were 93000 quadratic tetrahedral stress elements in model. The Mori-Tanaka homogenisation scheme and exterior point Eshelby solution were used in the micromechanical solution. Figure 4 compares the numerical and analytical major principal stresses along section B-B. Again, the principal stresses recorded for both the micromechanical model and FE model compare favourably. These micromechanical and FE

comparisons are sufficiently close to provide confidence in the homogenisation scheme for the present work.

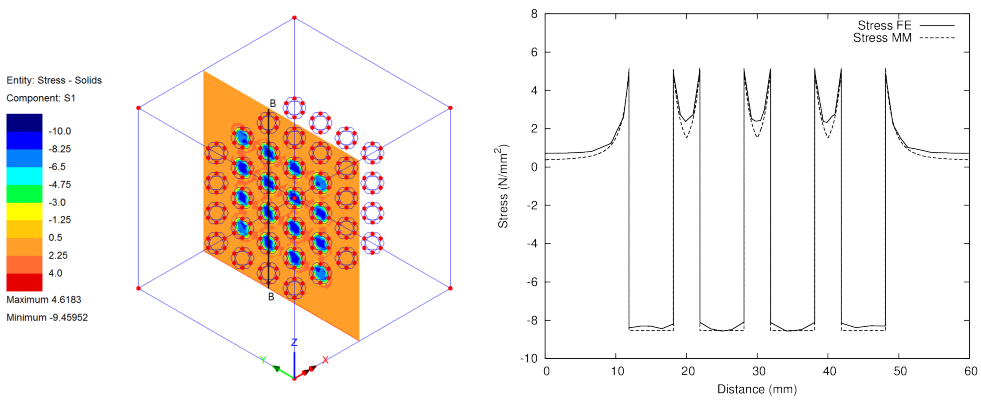

Figure 4: 3D FE plot and stress spatial distribution plot for multi-inclusion

5. Numerical implementation

The constitutive model presented above has been implemented in a Mathcad (2010) sheet using a constitutive driver algorithm. The model can be driven by total stress ($\bar{\boldsymbol{\sigma}}$), total strain ($\bar{\boldsymbol{\varepsilon}}$) or the shrinkage potential of the matrix ($\boldsymbol{\varepsilon}_{shr}$). Table 2 shows the essential steps of the computational algorithm with a specified stress path increment ($\Delta\boldsymbol{\sigma}_a$) and applied shrinkage strain increment ($\Delta\boldsymbol{\varepsilon}_{shr}$) in the matrix only. Material data and initial conditions are read along with initial stress and strain parameters.

In Section 6, a selected set of stress/strain paths are used to present the characteristic response of the model. Section 7 considers shrinkage of a cementitious composite and compares model predictions with experimental data.

Table 2: Computational algorithm for specified stress path with matrix shrinkage

Enter with $\bar{\boldsymbol{\varepsilon}}_{prv}$, ζ_{Mprv}, ζ_{prv}, $\Delta\boldsymbol{\varepsilon}_{shr}$	Enter with strains and previous equivalent strain parameters
$\Delta\boldsymbol{\sigma} = \Delta\boldsymbol{\sigma}_a - \mathbf{D}_{Sec}\Delta\boldsymbol{\varepsilon}_{shr}$	Compute out of balance stresses
$\bar{\boldsymbol{\varepsilon}} = \bar{\boldsymbol{\varepsilon}} + \Delta\boldsymbol{\varepsilon}, \quad \bar{\boldsymbol{\sigma}} = \bar{\boldsymbol{\sigma}} + \Delta\boldsymbol{\sigma}_{rc}$	Update strains and stresses
Volumetric micro-crack component	
If $\sigma_{Mm} \leq f_{tm}$ then $\omega_M = 0$	Micro-crack initiation condition
Else	Volumetric micro-crack evolution
$\zeta_M = \varepsilon_M - \varepsilon_{shr}$ if $\zeta_M > \zeta_{Mprv}$	Update strain parameter if it exceeds previous maximum
Update ω_M	Update damage parameter
End	
Directional micro-crack components	
For $id = 1$ to n_{id}	Loop over integration directions
$\boldsymbol{\varepsilon}_{M\Omega} = \mathbf{T}_{E\omega_M}(\mathbf{x}) : \boldsymbol{\varepsilon}_M - \mathbf{T}_{\Omega\omega_M} \cdot \mathbf{S}_E(\mathbf{x}) : \boldsymbol{\varepsilon}_{shr}$	Compute average matrix stress at peak position (EPE)
$s_{M\Omega} = \mathbf{N}_{id} \cdot \mathbf{D}_{M\omega} : (\boldsymbol{\varepsilon}_{M\Omega} - \boldsymbol{\varepsilon}_{shr})$	Compute local cracking stress at peak position
If $s_I(s_{M\Omega})_{max} \leq f_{td}$ then $\omega_{id} = 0$	Micro-crack initiation criterion
Else	Directional micro-crack evolution
$\boldsymbol{\varepsilon}_{L_{id}} = (1-\omega_{id})\mathbf{C}_{LM} : s_{m\Omega} + \omega_{id}\mathbf{N}_{\varepsilon_{id}} \cdot \bar{\boldsymbol{\varepsilon}}$	Evaluate local strain vector
$\zeta_{id} = f_d(\boldsymbol{\varepsilon}_{L_{id}})$ if $\boldsymbol{\varepsilon}_{L_{id}} > \zeta_{prv_{id}}$	Update strain parameter if exceeds previous max
Update ω_{id}	Update damage parameter
End	
$\mathbf{C}_{add} = \sum_{id=1}^{n_{id}} \mathbf{N}_{\varepsilon_{id}} \cdot \mathbf{C}_L \cdot \mathbf{N}_{id} \cdot \frac{\omega_{id}}{1-\omega_{id}} \mathsf{w}_{id}$	Evaluate total added compliance
$\mathbf{D}_{Sec} = \left(\mathbf{I}^{4s} + \mathbf{D}_{M\Omega\omega_M} \cdot \mathbf{C}_{add}\right)^{-1} \cdot \mathbf{D}_{M\Omega\omega_M}$	Form secant constitutive matrix
$\bar{\boldsymbol{\sigma}} = \mathbf{D}_{Sec} : (\bar{\boldsymbol{\varepsilon}} - \boldsymbol{\varepsilon}_{INEQ\omega_M})$	Compute stresses

6. Characteristic model predictions

A series of stress-strain paths are used to illustrate the characteristic response of the model. The paths selected are as follows;

1. Time dependent matrix shrinkage with and without associated matrix micro-cracking.
2. Matrix shrinkage restrained uniaxially with and without micro-cracking.
3. A uniaxial tensile strain path with and without matrix shrinkage.
4. Matrix shrinkage during the Willam et al. (1987) strain path which involves micro-crack formation under uniaxial tension followed by a rotating principal strain path.

The material properties are presented in Table 3 and are typical for a standard strength concrete. The inelastic strain applied in the matrix in all of the stress-strain paths is derived from the drying shrinkage strain from the EC2 code of practice (EN1992, 2008). The results are presented in graphical form showing the response for each path in terms of composite average stress and strain components.

Table 3: Typical cementitious composite material properties

f_M	E_M (N/mm^2)	ν_M	f_Ω	E_Ω (N/mm^2)	ν_Ω	ε_{od}	f_{td} (N/mm^2)	ε_{om}	f_{tm} (N/mm^2)
0.3	20000	0.15	0.7	55000	0.25	0.0067	2	0.01	1.33

Path 1 simulates free shrinkage of the composite, for which the mean composite stress remains null. The results for simulations with and without

micro-cracking (denoted MC and NMC respectively) are given in Figures 5b and 5c. These graphs provide the separate responses of the phases and show that the inclusion of micro-cracking in the model has a very significant effect on the stresses within the phases.

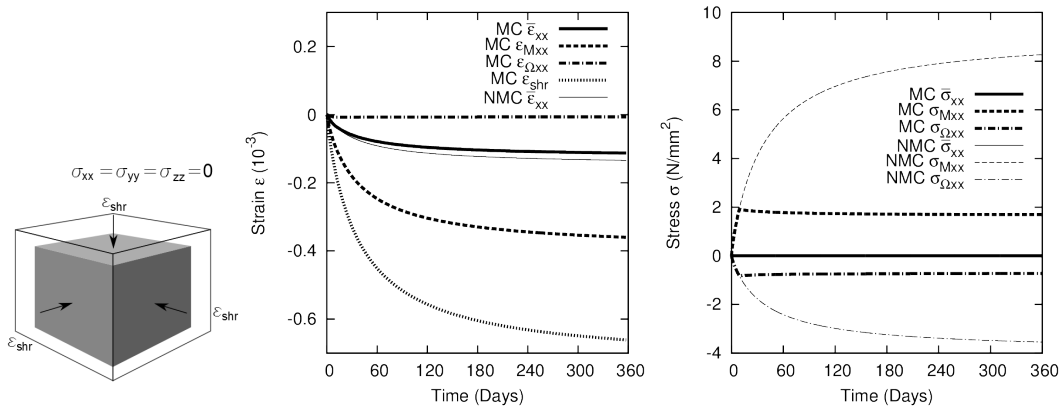

(a) Path 1 (b) Strain (c) Stress

Figure 5: Time dependent matrix shrinkage with and without associated matrix micro-cracking

Path 2 simulates the behaviour in a restrained structural component. In this path, the composite xx strain component is fixed at zero and all other composite strain components are unrestrained. The results are given in Figures 6a to 6c and again illustrate the importance of micro-cracking on the response of the phases.

Path 3 shows a uniaxial strain path with shrinkage strain (SS) in the matrix and without shrinkage strain (NSS) in the matrix. Figures 7a and 7b show the control data and strain loading paths. The stress results in figure 7c show that the peak stress in the SS case is 7% greater than in the NSS. The

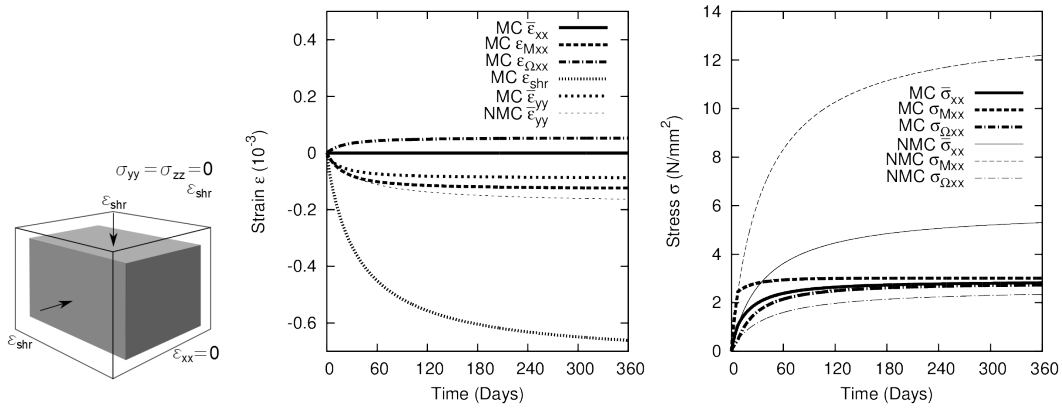

(a) Path 2 (b) Strain (c) Stress

Figure 6: Matrix shrinkage restrained uniaxially with and without micro-cracking

individual matrix and inclusion stresses have been omitted from the figures for clarity.

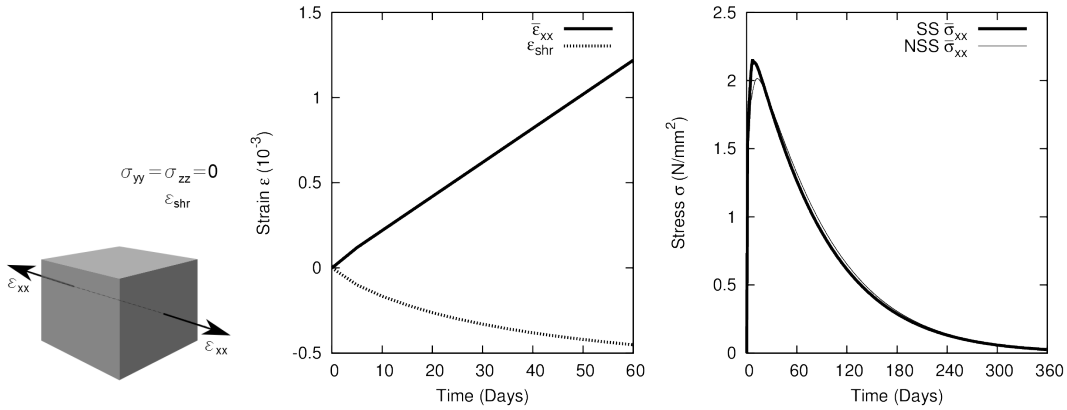

(a) Path 3 (b) Strain (c) Stress

Figure 7: An uniaxial tensile strain path with and without matrix shrinkage

Figures 8a to 8c illustrate the input for Path 4. The stress plots in Figure 8d compare the rotating stress response with the uniaxial stress response (US) without any rotation strains and correctly shows degradation of strength in the lateral direction with rotation. Figure 8e shows that the major principal stress decreases as the shear strain increases, as is desirable (Willam et al., 1987).

These paths illustrate the response of the model for a range of paths with and without micro-cracking and matrix shrinkage. The responses are all considered to be reasonable and to show that the two micro-cracking model components work together seamlessly.

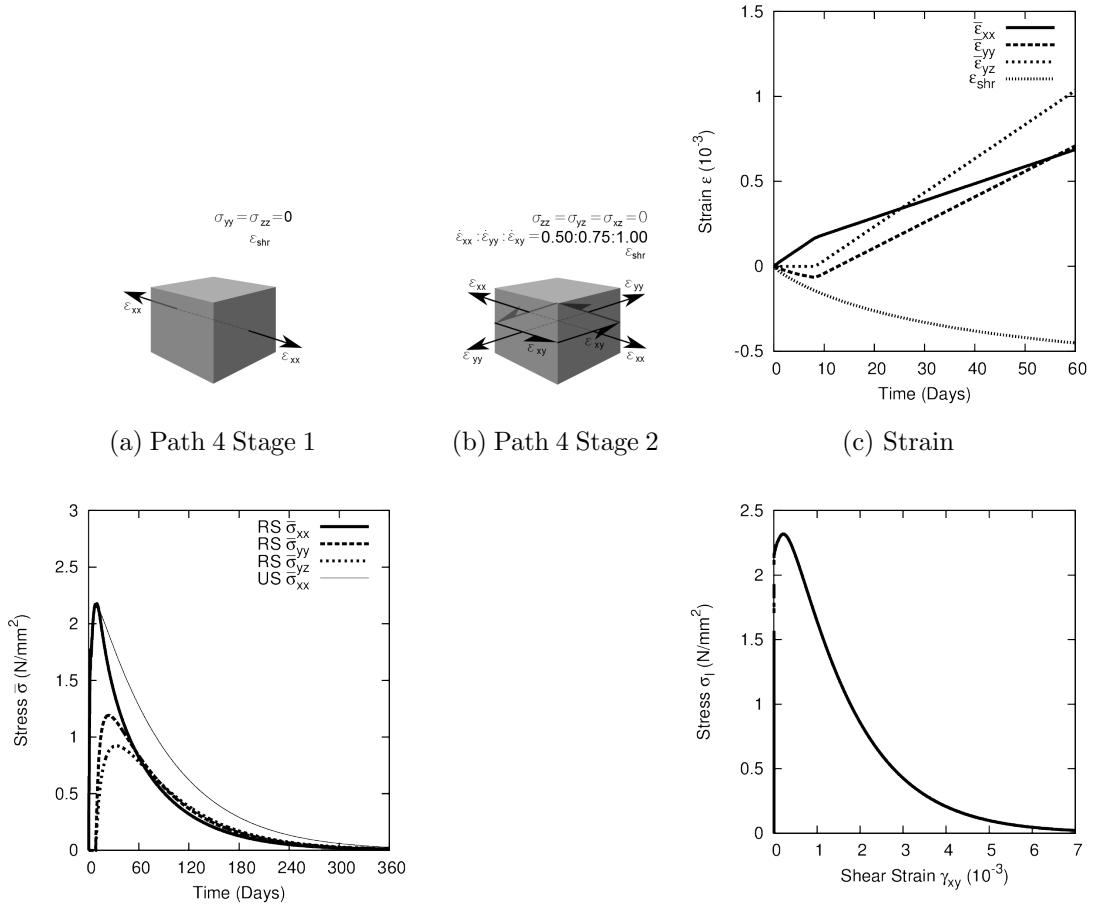

(a) Path 4 Stage 1 (b) Path 4 Stage 2 (c) Strain

(d) Stress (e) Principal stress and shear strain

Figure 8: Matrix shrinkage during the Willam et al. (1987) strain path which involves micro-crack formation under uniaxial tension followed by a rotating principal strain path

7. Autogenous shrinkage of a cementitious composite

In a cementitious composite material curing, creep and shrinkage occur mainly in the matrix phase whilst the aggregate phase tends to restrain ma-

trix movements. Most constitutive models for concrete creep and shrinkage consider the material as a whole e.g. (Neville et al., 1983; Bazant, 1995; Benboudjema et al., 2001, 2005; EN1992, 2008) and do not explicitly consider the separate behaviour of the phases. This means that material parameters for these empirically derived models must be generated for each mix. In this section an alternative approach is explored in which the model described above is applied to the problem of autogenous shrinkage of a cementitious composite. The aim is not to derive a comprehensive two-phase time dependent model for composite materials but rather to illustrate the benefits of applying the present model to such a problem. There have been a number of two-phase models for creep and shrinkage in concrete, for example Hirsch (1962), Counto (1964), England (1965) and Scheiner et al. (2009), see also Neville et al. (1983), but these do not explicitly consider the effects of micro-cracking. The present model is intermediate in complexity between the 4 level model of Pichler et al. (2007) and a single phase empirically based model, such as Bazant's B3 model (1995), although it is noted that the former model does not explicitly allow for the evolution of micro-cracks.

The objective of the following derivation is to produce a single shrinkage strain expression for a composite, given the properties of the matrix and inclusions as well as a shrinkage response for the matrix alone. To allow comparison with experimental results, a hydration model (Schindler and Folliard, 2005) is also included (see Appendix A) and implemented with a two-phase solidification model based on the solidifying material forming in a stress free state (Bazant and Prasannan, 1989). An autogenous free shrinkage problem is simulated using a volumetric solution with inelastic shrinkage strain in the

matrix (cement paste).

In the present approach, solidification strains (ε_s) are evaluated explicitly and these are defined as the inelastic strains necessary to ensure that solidified material first forms in a stress-free state. These strains are evaluated for each phase of the composite material by summing the increments associated with a change of solidified volume (Δv) that occurs over a step interval Δt. The expressions for the volumetric solidified strain increments for the matrix and inclusion phases are given in equations (35) and (36).

$$\Delta\varepsilon_{sM} = (v + \Delta v)^{-1} \Delta v \left(\varepsilon_M - \varepsilon_{shrM} - \varepsilon_{sM}\right) \tag{35}$$

$$\Delta\varepsilon_{s\Omega} = \left(T_{\Omega_v} S_\Omega + T_{\Omega_{\Delta v}} S_\Omega\right)^{-1} T_{\Omega_{\Delta v}} \left(\varepsilon_M - S_\Omega \left(\varepsilon_{shrM} + \varepsilon_{s\Omega}\right)\right) \tag{36}$$

The derivation of these expressions is given in Appendix B. In the present work, the hydration model of Schindler and Folliard (2005) is used to evaluate the degree of hydration over time and then the solidified volume is evaluated as a function of the degree of hydration using the assumption that the elastic modulus of the matrix phase is directly proportional to v. The relationship between the degree of hydration and the elastic modulus is established using the work of De Schutter (2002). Details of the hydration and solidification models are provided in Appendices A and B.

The mean composite stress in the material for a free shrinkage case is zero which results in the relationship between the total shrinkage in the composite and the shrinkage in the cement paste given in equation (37). The separate components of the solidification strains are accumulated over time and thus remain explicit in the expression.

$$\bar{\varepsilon} = -f_\Omega T_{\Omega_v} S_\Omega \left(\varepsilon_{shrM} + \varepsilon_{s\Omega}\right) + \tag{37}$$

$$K_{M\Omega v}^{-1} f_M K_{Mv} \left(\varepsilon_{shrM} + \varepsilon_{sM}\right) +$$

$$K_{M\Omega v}^{-1} f_\Omega K_\Omega T_{\Omega_v} S_\Omega \left(\varepsilon_{shrM} + \varepsilon_{s\Omega}\right)$$

ε_{shrM} is the matrix shrinkage strain, ε_{sM} is the solidification strain in the matrix and $\varepsilon_{s\Omega}$ is the solidification strain in the inclusion. The scalar values T_{Ω_v}, S_Ω, $A_{\Omega v}$ and $K_{M\Omega v}$ are given by the following equations.

$$T_{\Omega_v} = (1 + S_\Omega \cdot A_{\Omega v}) \tag{38}$$

$$S_\Omega = \frac{1}{3} \cdot \frac{(\nu_M + 1)}{(1 - \nu_M)} \tag{39}$$

$$A_{\Omega v} = \left[(K_\Omega - K_{Mv}) \cdot S_\Omega + K_{Mv}\right]^{-1} \cdot (K_{Mv} - K_\Omega) \tag{40}$$

$$K_{M\Omega v} = \left(f_M K_{Mv} + K_\Omega T_{\Omega_v}\right) \left(f_\Omega T_{\Omega_v} + f_M\right)^{-1} \tag{41}$$

Two examples are now used to illustrate the model performance with and without micro-cracking; (i) considers the experimental data of Pickett (1956) where the shrinkage of concrete with different volumetric proportions of aggregate were tested and (ii) comparing model results with shrinkage test data from Baroghel-Bouny (1994). In both cases, the cement paste shrinkage experimental results have been used to drive the volumetric free shrinkage for the concrete model. Key model parameters used are shown in Tables 4 and 5. For the Pickett (1956) data, Ottawa sand, type 1 cement and 0.35 W/C ratio were used. The model results are compared to the experimental results with micro-cracking (MC) and without micro-cracking (NMC).

Figure 9 and 10 show results without micro-cracking and with volumetric micro-cracking. It can be seen, in both cases, micro-cracking brings the strain results closer to the experimental findings. The difference between the

Table 4: Typical cementitious composite material properties Pickett (1956)

f_M	E_M (N/mm^2)	ν_M	f_Ω	E_Ω (N/mm^2)	ν_Ω	E	ε_{om}	f_{tm} (N/mm^2)
0.338	12600	0.2	0.662	60000	0.25	28600	0.0375	1.0

Table 5: Typical cementitious composite material properties Baroghel-Bouny (1994)

f_M	E_M (N/mm^2)	ν_M	f_Ω	E_Ω (N/mm^2)	ν_Ω	E	ε_{om}	f_{tm} (N/mm^2)
0.213	25500	0.25	0.787	55000	0.3	48707	0.0563	0.67

analytical solution and the experimental results without micro-cracking is 8.3% for Pickett (1956) and 18.0% for Baroghel-Bouny (1994). With micro-cracking the difference is 2.6% for Pickett (1956) and 4.4% for Baroghel-Bouny (1994).

In addition to comparing with experimental results, this volumetric model has been subjected to a parametric study. The hydration model is based on a type II cement with shrinkage strain taken from EC2 code of practice (EN1992, 2008) and with fixed micro-cracking parameters. The composition (volume fraction of aggregate f_Ω) and elastic modulus have been varied, and cases with and without micro-cracking considered as shown in Figure 11. As may be seen, micro-cracking is most pronounced when the matrix and inclusion volume fractions are equal. These plots suggest that the model could be used as a concrete design tool.

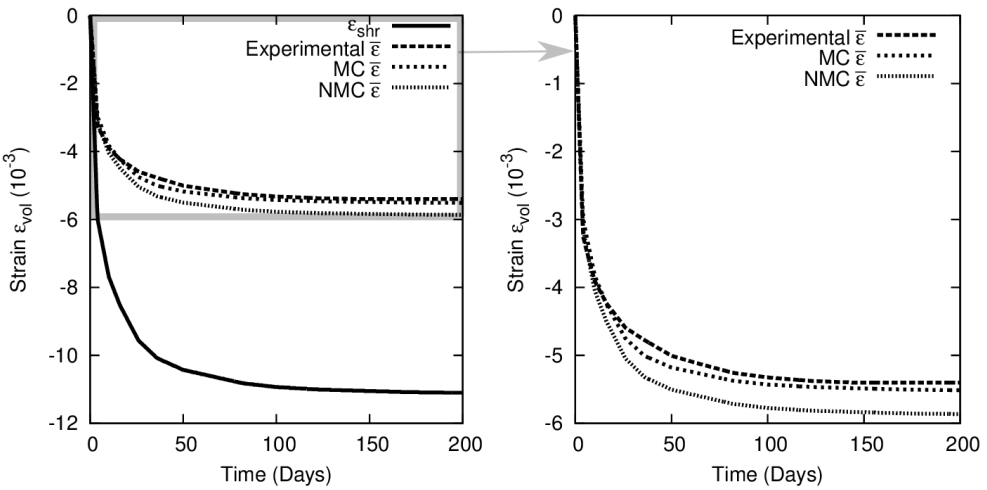

Figure 9: Pickett (1956) experimental results compared to model with and without micro-cracking

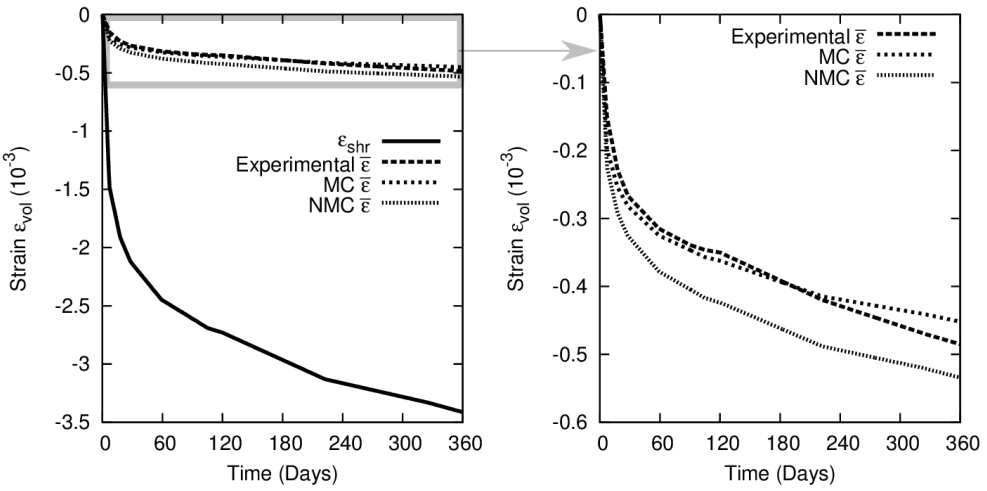

Figure 10: Baroghel-Bouny (1994) experimental results compared to model with and without micro-cracking

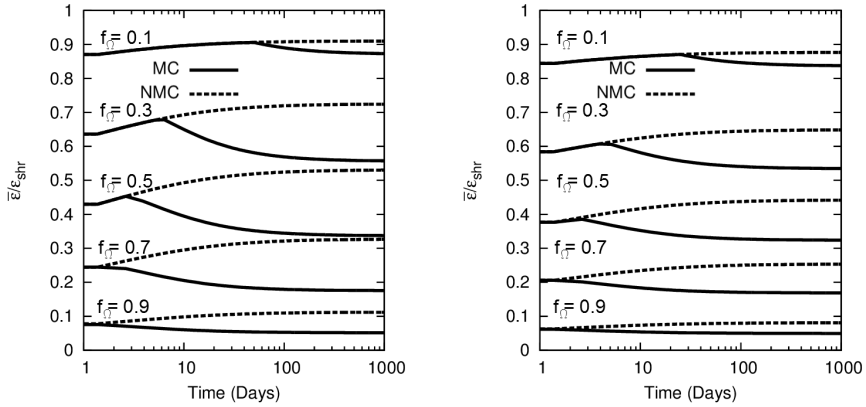

(a) Elastic modulus ratio $2E_M : E_\Omega$

(b) Elastic modulus ratio $E_M : E_\Omega$

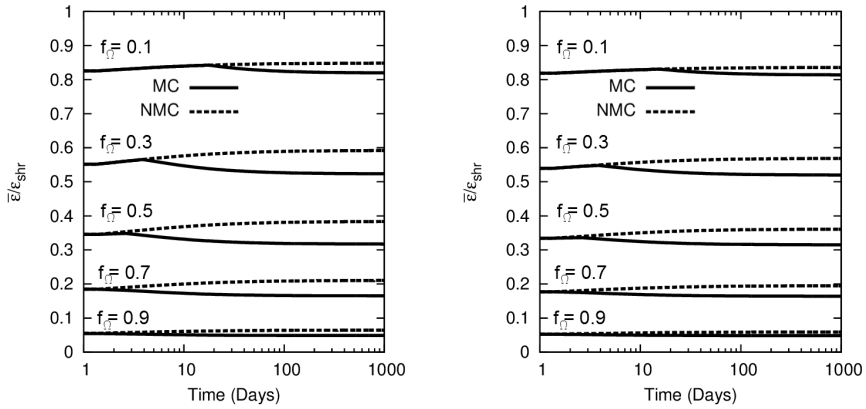

(c) Elastic modulus ratio $E_M : 2E_\Omega$

(d) Elastic modulus ratio $E_M : 3E_\Omega$

Figure 11: Parametric study of total shrinkage/matrix shrinkage with and without micro-cracking

8. Conclusions

- The proposed approach for homogenisation and the exterior point Eshelby expression used to simulate stress concentrations adjacent to inclusions are both valid for the case of matrix shrinkage; as shown in a series of finite element simulations in which inclusions were modelled explicitly.
- The combination of model components for isotropic matrix micro-cracking and directional (anisotropic) micro-cracking in the composite material allows early age volumetric and mechanically induced directional micro-cracking to be simulated in a computationally convenient manner.
- The model provides an accurate means for simulating the inelastic behaviour of concrete subject to autogenous drying and for quantifying the effects of micro-cracking during this drying process.

Acknowledgements

The writers would like to acknowledge the support of their industrial sponsors LUSAS, Alun Griffiths Contractors Ltd and Cardiff University's President Scholarship for the opportunity to carry out this research.

9. Highlights

- New approach for matrix micro-cracking and time-dependent behaviour in a two-phase composite.
- 3D FE validation of homogenisation and exterior point Eshelby solution for matrix shrinkage.

- Separation of isotropic and anisotropic micro-cracking components.
- Example stress-strain paths to illustrate model characteristics.
- Inelastic behaviour of concrete subject to autogenous drying is successfully simulated.

Appendix A. Hydration model

The relative degree of hydration of the cement with time is based on the work of Schindler and Folliard (2005). The total heat of hydration (H_{cem} inJ/g) for cement is calculated using the fraction by weight (p_i) for the different cement components of the total cement (p_{cem}).

$$H_{cem} = 500p_{C_3S} + 260p_{C_2S} + 866p_{C_3A} + 420p_{C_4AF} + 624p_{SO_3} \tag{A.1}$$

$$+1186p_{FreeCaO} + 850p_{MgO}$$

The total heat of hydration(H_u) is calculated taking account of all the cementitious materials: Cement (cem), slag ($slag$), fly ash (FA).

$$H_u = H_{cem} \cdot p_{cem} + H_{slag} \cdot p_{slag} + H_{FA} \cdot p_{FA} \tag{A.2}$$

where, H_{slag} and H_{FA} are the heat of hydration of slag and fly ash respectively. The ultimate heat of hydration is calculated from

$$H_{uls} = H_u \cdot C_{cem} \tag{A.3}$$

where C_{cem} is the cementitious materials content. The relative degree of hydration (Γ_r) is given by equation (A.4).

$$\Gamma_r = exp\left(1 - \left(\frac{\tau}{t_e}\right)^{\beta}\right) \tag{A.4}$$

Where, τ is hydration time parameter and β is a hydration shape factor. t_e is the equivalent maturity or age and defined as follows.

$$t_e = \sum_{0}^{t} exp\left(\frac{A_E}{R}\left(\frac{1}{T_r} - \frac{1}{T_c}\right)\right) \cdot \Delta t \tag{A.5}$$

Where A_E is the activation energy, R is the universal gas constant, T_r and T_c are the reference and current temperatures respectively. The rate of heat generation is also given by Schindler and Folliard (2005) but not used in this work. The expressions proposed in this hydration model are therefore;

$$v = {\Gamma_r}^{c_E} \tag{A.6}$$

$$E\left(\Gamma_r\right) = {\Gamma_r}^{c_E} \cdot E_f = v \cdot E_f \tag{A.7}$$

$$f_c\left(\Gamma_r\right) = {\Gamma_r}^{c_{f_c}} \cdot f_{cf} \tag{A.8}$$

$$f_t\left(\Gamma_r\right) = {\Gamma_r}^{c_{f_t}} \cdot f_{tf} \tag{A.9}$$

with c_E taken as 0.7 from De Schutter (2002) also implemented in the solidification theory. c_{f_c} and c_{f_t} are taken as 1.5 and 1.0, matching data from Yi et al. (2003). The definition of Γ_r is different from that employed by De Schutter, in that the present expression doesnt include a percolation threshold value of Γ. Our approach is to assume that the stress is zero up to a certain degree of hydration (Γ_c), which is typically taken to be 0.35, with the zero stress state being maintained via solidification strains.

The data used in the hydration model to simulate the data of Pickett (1956) and Baroghel-Bouny (1994) are shown in Tables A.6 and A.7 respectively.

Table A.6: Hydration model parameters used for Pickett (1956)

p_{C_3S}	p_{C_2S}	p_{C_3A}	p_{C_4AF}	p_{SO_3}	$p_{FreeCaO}$	p_{MgO}	p_{cem}	Blaine (m^2/kg)	C_{cem} (kg/m^3)
0.565	0.140	0.100	0.080	0.035	0.029	0.013	1	350	400

Table A.7: Hydration model parameters used for Baroghel-Bouny (1994)

p_{C_3S}	p_{C_2S}	p_{C_3A}	p_{C_4AF}	p_{SO_3}	$p_{FreeCaO}$	p_{MgO}	p_{cem}	Blaine (m^2/kg)	C_{cem} (kg/m^3)
0.573	0.240	0.030	0.076	0.020	0.053	0.008	1	312	400

Appendix B. Solidification model

The degree of hydration is related to the solidified volume (v) of material according to Equation (A.6). Working in volumetric terms and including volumetric micro-cracking, the bulk modulus of the inclusion is K_Ω and matrix is as follows.

$$K_{Mv} = (1 - \omega_M) \cdot v \cdot K_M \tag{B.1}$$

The notation referring to micro-cracking in the matrix is not included for clarity. If the volume of solidified material increases by Δv the damaged bulk modulus becomes

$$K_{M(v+\Delta v)} = (1 - \omega_M) \cdot (v + \Delta v) \cdot K_M = K_{Mv} + K_{M\Delta v} \tag{B.2}$$

Appendix B.1. Solidification

The stress in the matrix material before solidification is

$$\sigma_M = K_{Mv} \left(\varepsilon_M - \varepsilon_{shrM} - \varepsilon_{sM} \right) \tag{B.3}$$

Bazants solidification theory states that material should form in a stress free state, thus there should be no change of stress due to an increment of solidification alone. i.e. $\Delta\sigma_{M\Delta v} = 0$.

$$\sigma_M + \Delta\sigma_{M\Delta v} = K_{M(v+\Delta v)} \left(\varepsilon_M - \varepsilon_{shrM} - \varepsilon_{sM} - \Delta\varepsilon_{sM} \right) \tag{B.4}$$

Therefore,

$$\Delta\sigma_{M\Delta v} = -K_{Mv}\Delta\varepsilon_{sM} + K_{M\Delta v} \left(\varepsilon_M - \varepsilon_{shrM} - \varepsilon_{sM} - \Delta\varepsilon_{sM} \right) = 0 \tag{B.5}$$

which can be rearranged to provide the change in solidification strain in the matrix.

$$\Delta\varepsilon_{sM} = (v + \Delta v)^{-1} \Delta v \cdot \left(\varepsilon_M - \varepsilon_{shrM} - \varepsilon_{sM} \right) \tag{B.6}$$

Similarly, the stress in the inclusion before solidification of the matrix is given by,

$$\sigma_\Omega = K_\Omega T_{\Omega v} \left(\varepsilon_M - S_\Omega \left(\varepsilon_{shrM} + \varepsilon_{s\Omega} \right) \right) \tag{B.7}$$

Upon solidification there is no change in stress in the inclusion. i.e. $\Delta\sigma_{\Omega\Delta v} = 0$

$$\sigma_\Omega + \Delta\sigma_{\Omega\Delta v} = K_\Omega T_{\Omega(v+\Delta v)} \left(\varepsilon_M - S_\Omega \left(\varepsilon_{shrM} + \varepsilon_{s\Omega} + \Delta\varepsilon_{s\Omega} \right) \right) \tag{B.8}$$

Therefore,

$$\Delta\sigma_{\Omega\Delta v} = -K_\Omega T_{\Omega v} S_\Omega \Delta\varepsilon_{s\Omega} + K_\Omega T_{\Omega\Delta v} \left(\varepsilon_M - S_\Omega \left(\varepsilon_{shrM} + \varepsilon_{s\Omega} + \Delta\varepsilon_{s\Omega} \right) \right) = 0 \tag{B.9}$$

which can be rearranged to provide the change in solidification strain in the inclusion.

$$\Delta\varepsilon_{s\Omega} = \left(T_{\Omega v} S_\Omega + T_{\Omega\Delta v} S_\Omega\right)^{-1} T_{\Omega\Delta v} \cdot \left(\varepsilon_M - S_\Omega \left(\varepsilon_{shrM} + \varepsilon_{s\Omega}\right)\right) \tag{B.10}$$

Where $T_{\Omega\Delta v} = T_{\Omega(v+\Delta v)} - T_{\Omega v}$ is calculated explicitly.

$$T_{\Omega_v} = \left(1 + S_\Omega \cdot A_{\Omega v}\right) \tag{B.11}$$

$$A_{\Omega v} = \left[\left(K_\Omega - K_{Mv}\right) \cdot S_\Omega + K_{Mv}\right]^{-1} \cdot \left(K_{Mv} - K_\Omega\right) \tag{B.12}$$

$$T_{\Omega(v+\Delta v)} = \left(1 + S_\Omega \cdot A_{\Omega(v+\Delta v)}\right) \tag{B.13}$$

$$A_{\Omega(v+\Delta v)} = \left[\left(K_\Omega - K_{M(v+\Delta v)}\right) \cdot S_\Omega + K_{M(v+\Delta v)}\right]^{-1} \cdot \left(K_{M(v+\Delta v)} - K_\Omega\right) \tag{B.14}$$

Appendix B.2. Solidification in composite

For total stress equation upon solidification is defined by the following equation,

$$\bar{\sigma} = f_M \cdot \left(\sigma_M + \Delta\sigma_M\right) + f_\Omega \cdot \left(\sigma_\Omega + \Delta\sigma_\Omega\right) \tag{B.15}$$

which upon substitution becomes,

$$\bar{\sigma} = f_M K_{M(v+\Delta v)} \left(\boldsymbol{\varepsilon}_M - \boldsymbol{\varepsilon}_{shrM} - \boldsymbol{\varepsilon}_{sM} - \Delta\boldsymbol{\varepsilon}_{sM}\right) + \tag{B.16}$$

$$f_\Omega K_\Omega T_{\Omega(v+\Delta v)} \left(\varepsilon_M - S_\Omega \left(\varepsilon_{shrM} + \varepsilon_{s\Omega} + \Delta\varepsilon_{s\Omega}\right)\right)$$

Total strain equation upon solidification,

$$\bar{\varepsilon} = f_\Omega \cdot T_{\Omega(v+\Delta v)} \left(\varepsilon_M - S_\Omega \left(\varepsilon_{shrM} + \varepsilon_{s\Omega} + \Delta\varepsilon_{s\Omega}\right)\right) + f_M \cdot \varepsilon_M \tag{B.17}$$

The overall constitutive relationship is therefore given by equation B.18.

$$\bar{\sigma} = K_{M\Omega(v+\Delta v)} \cdot \left(\bar{\varepsilon} - \varepsilon_{INEQ_{v+\Delta v}}\right) \tag{B.18}$$

where

$$K_{M\Omega(v+\Delta v)} = \left(f_M K_{M(v+\Delta v)} + K_\Omega T_{\Omega(v+\Delta v)}\right)\left(f_\Omega T_{\Omega(v+\Delta v)} + f_M\right)^{-1} \quad \text{(B.19)}$$

and

$$\begin{aligned} \varepsilon_{INEQ_{v+\Delta v}} = & -f_\Omega T_{\Omega(v+\Delta v)} S_\Omega \left(\varepsilon_{shrM} + \varepsilon_{s\Omega} + \Delta\boldsymbol{\varepsilon}_{s\Omega}\right) + \\ & K^{-1}_{M\Omega(v+\Delta v)} f_M K_{M(v+\Delta v)} \left(\varepsilon_{shrM} + \varepsilon_{sM} + \Delta\varepsilon_{sM}\right) + \\ & K^{-1}_{M\Omega(v+\Delta v)} f_\Omega K_\Omega T_{\Omega(v+\Delta v)} S_\Omega \left(\varepsilon_{shrM} + \varepsilon_{s\Omega} + \Delta\varepsilon_{s\Omega}\right) \end{aligned} \quad \text{(B.20)}$$

For free shrinkage $\bar{\varepsilon} = \varepsilon_{INEQ_{v+\Delta v}}$. It is noted that the Eshelby terms, S_Ω and T_Ω are volumetric and as such are reduced to scalars.

Nomenclature

$\mathbf{A}_\Omega$ As defined

$\mathbf{A}_{\Omega\omega_M}$ As defined

$A_{\Omega v}$ As defined

a Radius of the spherical inclusion

A_E Activation energy

$\mathbf{C}_{add}$ Total added compliance

$\mathbf{C}_L$ Elastic compliance

C_{cem} Cementitious material content

c_E Constants as defined

c_{f_c}	Constants as defined
c_{f_t}	Constants as defined
c	Evolution constant
$\mathbf{C}_{LM}$	Matrix compliance
$\mathbf{D}_M$	Matrix elastic tensor
$\mathbf{D}_{M\omega}$	Volumetric micro-cracked matrix tensor
$\mathbf{D}_{M\Omega}$	Composite elastic tensor
$\mathbf{D}_{M\Omega\omega_M}$	Volumetric micro-cracked composite tensor
$\mathbf{D}_{\Omega}$	Inclusion elastic tensor
E_{Ω}	Inclusion Youngs modulus
E_M	Matrix Young's modulus
E_d	Composite Young's modulus
f	Crack density parameter
F_{ζ_d}	Directional micro-cracking function
F_{ζ_m}	Volumetric micro-cracking function
f_M	Volume fraction matrix
f_{Ω}	Volume fraction inclusion

f_{td} Local directional tensile strength at the aggregate/ cement paste interface

f_{tm} Local volumetric tensile strength at the aggregate/ cement paste interface

H_{cem} Heat of hydration for cement

H_{FA} Heat of hydration for fly ash

H_{slag} Heat of hydration for slag

H_{uls} Ultimate heat of hydration

H_u Total heat of hydration

h_d description

h_m description

$\mathbf{I}^{4s}$ Fourth order identity tensor

K_M Bulk modulus of matrix

$K_{M\Omega v}$ Bulk modulus of composite

K_{Mv} Bulk modulus of matrix as a function of solidification

K_Ω Bulk modulus of inclusion

$\mathbf{N}$ Stress transformation tensor

$\mathbf{N}_\varepsilon$ Strain transformation tensor

n_{id}	Integration directions
p_{cem}	Total cement fraction
p_i	Fraction by weight of cement
R	Universal gas constant
r_{ζ_d}	As defined
r, s, t	Local coordinate system
$\mathbf{S}_E(\mathbf{x})$	Exterior point Eshelby tensor
$\mathbf{S}_\Omega$	Interior point fourth order Eshelby tensor
S_Ω	Volumetric interior point Eshelby tensor
s,$s_{M\Omega}$	Transformed amplified stress adjacent to inclusion
s_I	Local principal stress
$\mathbf{T}_{E\omega_M}(\mathbf{x})$	As defined
$\mathbf{T}_\Omega$	As defined
$\mathbf{T}_{\Omega\omega_M}$	As defined
T_{Ω_v}	As defined
T_c	Current temperature
t_e	Equivalent maturity or age
T_r	Reference temperature

u Relative displacement across a zone of material size equal to the coarse aggregate particles

u_{0d} Relative displacement for directional fully micro-cracked

u_{0m} Relative displacement for volumetric fully micro-cracked

v Solidified volume

$\mathbf{x}$ Position vector from the centre of a spherical aggregate particle

α_L As defined

$\bar{\boldsymbol{\varepsilon}}$ Composite average strain

$\boldsymbol{\varepsilon}_0$ Farfield strain

$\boldsymbol{\varepsilon}_\alpha$ Local additional strain tensor due to micro-cracking

$\boldsymbol{\varepsilon}_{INEQ\omega_M}$ As defined

$\boldsymbol{\varepsilon}_{INEQ}$ As defined

$\boldsymbol{\varepsilon}_{IN}$ Inelastic strain

$\boldsymbol{\varepsilon}_{M\Omega}$ Transformed amplified strain adjacent to inclusion

$\boldsymbol{\varepsilon}_M$ Matrix strain

ε_{0d} Local directional strains at effectively fully micro-cracked

ε_{0m} Local volumetric strains at effectively fully micro-cracked

$\varepsilon_{s\Omega}$ Inclusion solidification strain

ε_{shrM} Matrix shrinkage strain

ε_{sM} Matrix solidification strain

$\boldsymbol{\varepsilon}_a$ Total additional strain tensor due to micro-cracking

$\boldsymbol{\varepsilon}_c$ Disturbance strain

$\boldsymbol{\varepsilon}_L$ Local strain component

$\boldsymbol{\varepsilon}_{LMe}$ Peak elastic strain in the matrix

$\Delta\boldsymbol{\varepsilon}_{shr}$ Applied shrinkage strain increment

$\boldsymbol{\varepsilon}_{shr}$ Shrinkage potential of the matrix

ε_s Solidification strain

$\boldsymbol{\varepsilon}_\tau$ Eigenstrain

ε_{tm} Strain at first directional uniaxial micro-cracking

ε_{tm} Strain at first volumetric uniaxial micro-cracking

γ As defined

Γ_c Starting threshold degree of hydration

Γ_r Relative degree of hydration

γ_{xy} Shear strain x-y

ν_Ω Inclusion Poissons ratio

ν_M Matrix Poisson's ratio

ω_d	Directional micro-cracking parameter
ω_M	Volumetric micro-cracking parameter
ρ	Relative distance from the centre of a spherical aggregate particle
$\bar{\boldsymbol{\sigma}}$	Composite average stress
$\Delta\boldsymbol{\sigma}_{rc}$	Out of balance stress increment
σ_I	Principal strain
$\Delta\boldsymbol{\sigma}_a$	Stress path increment
$\boldsymbol{\sigma}_M$	Matrix stress
σ_{Mm}	Volumetric matrix stress
$\boldsymbol{\sigma}_\Omega$	Matrix stress
Δt	Time step interval
τ_L	As defined
Δv	Solidified volume increment
ζ_d	Directional effective local strain parameter
ζ_m	Volumetric effective local strain parameter
β	Subscript denoting denotes volumetric (m) or directional (d) micro-cracking
e	Subscript denoting elastic

M Subscript denoting matrix

Ω Subscript denoting inclusion

prv Subscript denoting previous time step

Δv Subscript denoting solidification increment

v, vol Subscript denotes volumetric

Acker, P., 2001. Micromechanical analysis of creep and shrinkage mechanisms. In: Creep, shrinkage and durability mechanics of concrete and other quasi-brittle materials. Proceedings of the sixth international conference (Concreep6).

Baroghel-Bouny, V., 1994. Characterization of cement pastes and concretes - methods, analysis, interpretations. Ph.D. thesis, Laboratoire Central des Ponts et Chausses, Paris.

Bazant, Z. P., 1995. Creep and shrinkage prediction model for analysis and design of concrete structures-model b3. Materials and Structures 28, 357–365.

Bazant, Z. P., Prasannan, S., 1989. Solidification theory for concrete creep: I. formulation. Journal of Engineering Mechanics 115 (8), 1691–1703.

Benboudjema, F., Meftah, F., Sellier, A., Torrenti, J. M., Heinfling, G., 2001. On the prediction of delayed strains for concrete subjected to drying and loading simultaneously. Proc. (CONCREEP) Creep, shrinkage and durability mechanics of concrete and other quasi-brittle materials 6, 245–250.

Benboudjema, F., Meftah, F., Torrenti, J. M., 2005. Interaction between drying, shrinkage, creep and cracking phenomena in concrete. Engineering structures 27 (2).

Benveniste, Y., Jun. 1987. A new approach to the application of Mori-Tanaka's theory in composite materials. Mechanics of Materials 6 (2), 147–157.

Bernard, O., Ulm, F. J., Lemarchand, E., 2003. A scale micromechanics-hydration model for the early-age elastic properties of cement-based materials. Cement and Concrete Research 33 (9), 1293–1309.

Budiansky, B., O'Connell, R., 1976. Elastic-moduli of a cracked solid. International Journal of Solids and Structures 12 (2), 81–97.

Carol, I., Rizzi, E., Willam, K., Jan. 2001. On the formulation of anisotropic elastic degradation. i. theory based on a pseudo-logarithmic damage tensor rate. International Journal of Solids and Structures 38 (4), 491–518.

Castaneda, P., Jun. 1996. Exact second-order estimates for the effective mechanical properties of nonlinear composite materials. Journal of the Mechanics and Physics of Solids 44 (6), 827–862.

Chaboche, J., Kruch, S., Maire, J., Pottier, T., 2001. Towards a micromechanics based inelastic and damage modeling of composites. International Journal of Plasticity 17 (4), 411–439.

Counto, U. J., 1964. The effect of the elastic modulus of the aggregate on the elastic modulus, creep and creep recovery of concrete. Magazine of

Concrete Research 16 (48), 129138.
URL http://www.icevirtuallibrary.com/content/article/10.1680/macr.1964.16.48.12

De Schutter, G., 2002. Finite element simulation of thermal cracking in massive hardening concrete elements using degree of hydration based material laws. Computers & Structures 80 (27-30), 20352042.

Desrumaux, F., Meraghni, F., Benzeggagh, M. L., Apr. 2001. Generalised mori-tanaka scheme to model anisotropic damage using numerical eshelby tensor. Journal of Composite Materials 35 (7), 603–624.

Dunn, M. L., Ledbetter, H., 1997. Elastic-plastic behavior of textured short-fiber composites. Acta materialia 45 (8), 3327–3340.

Dvorak, G. J., 1992. Transformation field analysis of inelastic composite materials. Proceedings of the Royal Society of London. Series A: Mathematical and Physical Sciences 437 (1900), 311.

Dvorak, G. J., Benveniste, Y., Aug. 1992. On transformation strains and uniform fields in multiphase elastic media. Proceedings of the Royal Society of London. Series A: Mathematical and Physical Sciences 437 (1900), 291–310.

EN1992, 2008. Eurocode 2 : Design of concrete structures : British standard. BSi, London.

England, G. L., 1965. Method of estimating creep and shrinkage strains in concrete from properties of constituent materials. In: ACI Journal Proceedings. Vol. 62. pp. 1411–1420.

Eshelby, J. D., 1957. The determination of the elastic field of an ellipsoidal inclusion, and related problems. Proceedings of the Royal Society of London. Series A, Mathematical and Physical Sciences, 376–396.

Grassl, P., Jirasek, M., 2006. Damage-plastic model for concrete failure. International journal of solids and structures 43 (22), 7166–7196.

Hearn, N., 1999. Effect of shrinkage and load-induced cracking on water permeability of concrete. ACI Materials Journal 96 (2).

Hill, R., Apr. 1965. Continuum micro-mechanics of elastoplastic polycrystals. Journal of the Mechanics and Physics of Solids 13 (2), 89–101.

Hirsch, T. J., 1962. Modulus of elasticity iof concrete affected by elastic moduli of cement paste matrix and aggregate. In: ACI Journal Proceedings. Vol. 59 of 3. pp. 427–451.

Jefferson, A. D., Bennett, T., 2007. Micro-mechanical damage and rough crack closure in cementitious composite materials. International Journal for Numerical and Analytical Methods in Geomechanics 31 (2), 133–146.

Ju, J., Sun, L., Jan. 2001. Effective elastoplastic behavior of metal matrix composites containing randomly located aligned spheroidal inhomogeneities. part i: micromechanics-based formulation. International Journal of Solids and Structures 38 (2), 183–201.

Ju, J. W., Sun, L. Z., Jun. 1999. A novel formulation for the exterior-point eshelbys tensor of an ellipsoidal inclusion. Journal of Applied Mechanics 66 (2), 570–574.

Laws, N., Jan. 1973. On the thermostatics of composite materials. Journal of the Mechanics and Physics of Solids 21 (1), 9–17.

Leukart, M., Ramm, E., Nov. 2003. A comparison of damage models formulated on different material scales. Computational Materials Science 28 (34), 749–762.

Leukart, M., Ramm, E., 2006. Identification and interpretation of microplane material laws. Journal of Engineering Mechanics 132 (3), 295–305.

LUSAS, 2012. LUSAS solver reference manual. 14.7 Issue 1.
URL http://www.lusas.com/

Mathcad, 2010. Mathcad help manual. 15.0.
URL http://www.ptc.com/product/mathcad/

Mihai, I., Jefferson, A., Dec. 2011. A material model for cementitious composite materials with an exterior point eshelby microcrack initiation criterion. International Journal of Solids and Structures 48, 3312–3325.

Monchiet, V., Gruescu, C., Cazacu, O., Kondo, D., 2012. A micromechanical approach of crack-induced damage in orthotropic media: application to a brittle matrix composite. Engineering Fracture Mechanics 83, 4053.

Mori, T., Tanaka, K., May 1973. Average stress in matrix and average elastic energy of materials with misfitting inclusions. Acta Metallurgica 21 (5), 571–574.

Mura, T., 1987. Micromechanics of defects in solids, 2nd Edition. M. Ni-

jhoff ;;Distributors for the U.S. and Canada Kluwer Academic Publishers, Dordrecht Netherlands ;Boston ;Hingham ;MA ;USA.

Nemat-Nasser, S., Hori, M., 1999. Micromechanics: overall properties of heterogeneous materials. Elsevier, Amsterdam; New York.

Neville, A. M., Dilger, W. H., Brooks, J. J., 1983. Creep of plain and structural concrete. Construction Press, London ; New York.

Pichler, B., Hellmich, C., May 2011. Upscaling quasi-brittle strength of cement paste and mortar: A multi-scale engineering mechanics model. Cement and Concrete Research 41 (5), 247–476.

Pichler, C., Lackner, R., 2008. A multiscale creep model as basis for simulation of earlyage concrete behavior. Computers and Concrete 5 (4), 295–328.

Pichler, C., Lackner, R., Mang, H. A., 2007. A multiscale micromechanics model for the autogenous-shrinkage deformation of early-age cement-based materials. Engineering fracture mechanics 74 (1-2), 34–58.

Pickett, G., 1956. Effect of aggregate on shrinkage of concrete and a hypothesis concerning shrinkage. In: ACI Journal Proceedings. Vol. 52.

Scheiner, S., Hellmich, C., et al., 2009. Continuum microviscoelasticity model for aging basic creep of early-age concrete. Journal of Engineering Mechanics 135, 307.

Schindler, A. K., Folliard, K. J., 2005. Heat of hydration models for cementitious materials. ACI materials journal 102 (1), 24–33.

Stroud, A., Apr. 1972. Approximate Calculation of Multiple Integrals. Prentice Hall.

Sun, C., Saffari, P., Ranade, R., Sadeghipour, K., Baran, G., Jan. 2007. Finite element analysis of elastic property bounds of a composite with randomly distributed particles. Composites Part A: Applied Science and Manufacturing 38 (1), 80–86.

Tandon, G. P., Weng, G. J., 1988. A theory of particle-reinforced plasticity. Journal of applied mechanics 55, 126.

van Mier, J. G. M., 1997. Fracture processes of concrete : Assessment of material parameters for fracture models. CRC Press, Boca Raton.

Walraven, J. C., Reinhardt, H. W., 1981. Concrete mechanics. part a: Theory and experiments on the mechanical behavior of cracks in plain and reinforced concrete subjected to shear loading. NASA STI/Recon Technical Report N 82, 25417.

Weng, G. J., 1988. Theoretical principles for the determination of two kinds of composite plasticity- inclusions plastic vs. matrix plastic. Mechanics of composite materials- 1988, 193–208.

Willam, K., Pramono, E., Sture, S., 1987. Fundemental issues of smeared crack models. pp. 192–207.

Xi, Y., Jennings, H. M., Jul. 1997. Shrinkage of cement paste and concrete modelled by a multiscale effective homogeneous theory. Materials and Structures 30 (6), 329–339.

Yi, S. T., Kim, J. K., Oh, T. K., 2003. Effect of strength and age on the stress-strain curves of concrete specimens. Cement and Concrete Research 33 (8), 1235–1244.